International Journal of Heat and Mass Transfer 52 (2009) 5557–5566

Contents lists available at ScienceDirect

International Journal of Heat and Mass Transfer

journal homepage: www.elsevier.com/locate/ijhmt

Modeling of nucleate boiling heat transfer under an impinging free jet

A.M.T. Omar [a,b], M.S. Hamed [a,b,*], M. Shoukri [b]

[a] Thermal Processing Laboratory (TPL), McMaster University, Hamilton, Ont., Canada L8S 4L7
[b] Department of Mechanical Engineering, McMaster University, Hamilton, Ont., Canada L8S 4L7

ARTICLE INFO

Article history:
Received 2 October 2008
Received in revised form 17 June 2009
Accepted 17 June 2009
Available online 11 August 2009

Keywords:
Flow boiling
Jet impingement cooling
Bubble-induced mixing
Enhanced diffusivity
Modeling
Nucleate boiling

ABSTRACT

A model using an analytical/empirical approach has been developed to predict the rate of heat transfer in the stagnation region of a planar jet impinging on a horizontal flat surface. The model has been developed based on the hypothesis that bubble-induced mixing would result in enhanced or additional diffusivity. The additional diffusivity has been included in the diffusion term of the conservation equations. The value of the effective diffusivity has been correlated with jet parameters (velocity and temperature) and surface temperature using experimental data. The important aspects of the bubble dynamics (generation frequency and average bubble diameter) have been acquired using high-speed imaging and an intrusive optical probe. The applicability of the proposed model has been investigated under conditions of partial and fully-developed nucleate boiling. Experiments have been carried out using water at atmospheric pressure, mass flux in the range of 388–1649 kg/m^2 s, degree of sub-cooling in the range of 10–28 °C, and surface temperature in the range of 75–120 °C. Results showed that the proposed model is able to predict the surface heat flux with reasonable accuracy (+30% and −15%).

1. Introduction

Jet impingement cooling (JIC) has attracted a lot of attention in the last few decades due to its high heat removal capability using significantly less amount of coolant [1]. JIC has been widely used in the heat treatment of metal parts [2–6], electronic cooling [7,8], and emergency cooling of nuclear safety systems. Using evaporable liquids such as water, boiling is likely to occur when the surface temperature exceeds the coolant saturation temperature. Boiling, generally speaking, is associated with large rates of heat transfer because of the latent heat of evaporation; and because of the enhancement of the level of turbulence between the liquid and the solid surface. This enhancement is due to the mixing action associated with the cyclic nucleation, growth, and departure or collapse of vapour bubbles on the surface [4]. In the case of flow boiling, such as boiling under impinging jets, the interaction between the bubble dynamics and the jet hydrodynamics has significant effect on the rate of heat transfer. The common approach used to determine the rate of boiling heat transfer is by using a set of empirical equations that correlate the value of the surface heat flux or the heat transfer coefficient with the fluid properties, surface conditions, and flow conditions [1,9–11]. Although this approach is simple, these empirical correlations are developed solely using regression analysis to fit the experimental data. These correlations do not provide much insight into the underlying physical mechanisms involved in the boiling heat transfer problem [12]. The alternative approach is to use mechanistic models.

Generally speaking, a mechanistic model is usually based on the concept of surface heat flux partitioning, i.e., the assumption that the surface heat flux comprise of multiple components. These components are usually: (1) the amount of heat used for direct evaporation to generate the bubbles; (2) the amount of heat transferred through transient conduction to the liquid replacing the departing bubbles; and (3) the amount of heat transferred through the enhanced convection due to the wakes generated by the emerging bubbles into the liquid. All mechanistic models of boiling heat transfer rely on experimentally developed relations or sub-models. These relations are used to correlate between the bubble departure diameter and release frequency and the other flow and surface parameters. There have been a number of mechanistic models developed for the case of pool boiling [13,14] and for the case of parallel flow boiling [15,16]. In the latter case, the boiling heat transfer phenomenon is more complicated due to the strong coupling between the flow, the thermal field, and bubble dynamics.

Basu et.al. [15] investigated sub-cooled water flow boiling in a vertical rectangular conduit. They proposed a mechanistic model assuming that the rate of heat transfer is mainly due to liquid sensible heating and evaporation that takes place within the superheated liquid layer adjacent to the surface. Their results indicated that bubble mixing enhanced the rate of heat transfer due to forced convection by 30%.

* Corresponding author. Address: Thermal Processing Laboratory (TPL), McMaster University, Hamilton, Ont., Canada L8S 4L7. Tel.: +1 905 525 9140x26113; fax: +1 905 572 7944.
E-mail address: hamedm@mcmaster.ca (M.S. Hamed).

0017-9310/$ - see front matter © 2009 Published by Elsevier Ltd.
doi:10.1016/j.ijheatmasstransfer.2009.06.025

Nomenclature

Symbol	*Definition*
A_v	area fraction covered with vapor
C	constant used in Eq. (4)
c_p	specific heat (J/kg °C)
c_ε	constant in Eq. (10) for diffusivity decay
D (or d)	diameter (m)
F	frequency of bubble release (Hz)
G	water mass flux (kg/m^2 s)
h	heat transfer coefficient (W/m^2 °C)
h_{fg}	latent heat of vaporization (J/kg)
Ja	Jacob number
H_n	nozzle to heater distance (m)
k	thermal conductivity (W/m °C)
N	decay function of the additional diffusivity
n	number of active nucleation sites
P	pressure (N/m^2)
Pr	Prandtl number (ratio between the momentum diffusivity to thermal diffusivity)
q''	heat flux (W/m^2)
Re	Reynolds number
T	Temperature (°C)
ΔT	temperature difference (°C)
u	velocity component parallel to flow direction (x-direction)
v	velocity component normal to flow direction (y-direction)
V_j	jet velocity (m/s)
V_{tsh}	threshold voltage (Fig. 8) (V)
We	Weber number

Greek symbols

α	molecular thermal diffusivity (m^2/s)
δ	boundary layer thickness (m)
ε	additional diffusivity due to bubble generation (m^2/s)
ε^+	ratio of the bubble induced maximum total diffusivity to the molecular diffusivity (dimensionless)
η	dimensionless coordinate, y/δ
θ	dimensionless temperature difference: $(T - T_\infty)/(T_{sat} - T_\infty)$
ν	molecular kinematic diffusivity (m^2/s)
ρ	density (kg/m^3)
σ	surface tension (N/m)
φ	angle of contact (°)
ψ	stream function (m^2/s)
Ψ	dimensionless stream function ($= \psi\sqrt{C/\varepsilon_{max}}$)

Subscripts

∞	free stream condition
b	bubble
c	characteristic
ev	evaporation
exp	experimental
h	thermal energy
hyd	hydraulic
j	jet related value
l	liquid
m	momentum related quantity
max	maximum value
mod	modified
$model$	model predicted value
nb	nucleate boiling quantity
o	values at the stagnation ($x = 0$)
s	surface
sat	saturation
sp	single phase value
sub	sub-cooled
sup	superheat
t	turbulent
v	vapour
w	jet width
ε	related to bubble-induced diffusivity

Superscripts

$'$	first derivative
$''$	second derivative

None of the existing mechanistic models considered the case of boiling heat transfer under impinging jets, where the flow field is quite different from the case of parallel flow. Under an impinging jet, the velocity is normal to the surface at the stagnation zone. Downstream of the stagnation zone there is a parallel flow region where the hydrodynamic and thermal boundary layers are developing. Followed by a fully-developed flow region, where similarity solutions exist [3,17,18]. Such variations in the flow field do not exist in the case of pool boiling or parallel flow boiling. These variations in the velocity field are expected to have significant effects on the bubble dynamics. Therefore, the applicability of the mechanistic models developed for pool and parallel flow boiling for the case of impinging jet requires investigation.

Analytical models have also been used for boiling heat transfer [4,19,20]. This approach depends on the use of some assumptions to simplify the mathematical formulation of the problem and to introduce the effect of boiling heat transfer into the equations. Zumbrunnen [3] and Wang et al. [18] used analytical solutions for the case of single-phase heat transfer from laminar impinging jets. They developed some matching factors to allow them to use similarity solutions in the various regions of the flow field of the impinging jet [17,18].

Mikielewicz et al. [20] developed an analytical model for sub-cooled flow boiling under an impinging circular free jet. The model was developed for the case of fully-developed nucleate boiling. They introduced a *blowing* parameter to the convective terms of the momentum and energy equations in order to account for the additional normal velocity caused by the bubble growth. Although the radial distribution of the heat transfer coefficient was determined, no validation with experimental data was reported.

Timm et al. [4] developed an analytical model to predict the wall heat flux from a planar free jet impinging on a flat surface. They modified the diffusion terms in the momentum and energy equations by adding additional diffusivity due to bubble-induced diffusion. They considered only film boiling, and so, they assumed that the entire surface was covered with a continuous bubble layer. The ratio of the surface temperature and the saturation temperature was in the range of $5 < T_s/T_{sat} < 8$. They varied the jet velocity in the range of 3–11 m/s. Little effect of the jet velocity on the rate of heat transfer was found. They did not provide any details of the effect of the degree of sub-cooling.

The concept of bubble-induced diffusion assumes that, on top of the fluid molecular diffusivity, there is an additional diffusivity due to the bubble dynamics (growth, departure, and collapse). This concept is analogous to the concept of eddy diffusivity used in turbulence modeling [21]. The advantage of using this concept is that it can be easily implemented in the conservation equations and so all the details of the flow and thermal fields can be obtained by

solving these equations numerically [19]. In boiling flows, the typical time and length scales associated with bubble dynamics are in the order of $10^{-5} \sim 10^{-4}$ s and 10^{-4}–10^{-3} m, respectively [4,22]. This is why numerical simulations of boiling heat transfer are computationally expensive. However, using the concept of bubble-induced diffusion, the numerical simulations do not have to deal with these very small length and time scales, and so the cost of computations is significantly reduced. Again, this is analogous to the cost of solving turbulence problems using direct numerical simulation (DNS) compared with the cost of computations using the concept of eddy diffusivity (turbulence modeling).

Dhir et al. [23] carried out a numerical study to fully resolve the details of bubble nucleation in pool boiling using DNS. The locations of the nucleation sites had to be pre-defined and limited in number. Although good agreement with experimental data was achieved, the use of DNS in simulating boiling heat transfer problems is still in its early stages and has not been tested for real situations, where numerous nucleation sites are randomly present on the surface. The use of DNS in simulating boiling under impinging jets will be even more challenging.

Narumanchi et al. [24] used the commercial package FLUENT® to simulate boiling heat transfer from a uniformly heated chip exposed to a submerged circular jet. The correlations used for calculating the effect of bubble dynamics were taken from previous studies on parallel flow boiling.

The numerical simulation of sub-cooled flow boiling during free jet impingement involves two major tasks: (1) simulate phase change due to boiling and account for its effect on flow hydrodynamics and (2) resolve the interface between the liquid and the surrounding gas (air). The current study is an attempt to provide a simplified means to carry out task (1). The proposed model would allow one to account for the effect of bubble generation due to boiling on flow hydrodynamics and on wall heat flux without the need to resolve details of phase change. This is achievable by incorporating additional diffusivity to the conservation equations of the liquid flow. By using this approach, only the task of resolving free surface would be tackled in the simulation, which would significantly reduce the complexity and cost of computations.

2. Model problem

Fig. 1 illustrates the details of the velocity field of a planar free jet impinging on a horizontal surface. The rectangular nozzle is 1 mm wide and 8 mm deep into the page. As the water jet impinges on the heated surface, the jet is assumed to divert symmetrically about the stagnation line and continues parallel to the surface. When the surface temperature is well above the saturation temperature of the liquid, bubbles start to nucleate and grow on the surface. The adjacent region to the surface where bubbles nucleate is referred to here as the "bubbly layer". The thickness of bubbly layer is assumed equal to the bubble diameter, as shown in Fig. 2. Due to the cyclic bubble growth and departure, additional disturbances are induced into the main flow. Such disturbances will improve the heat transfer from the surface to the fluid bulk. For nucleation to take place within that layer there should be enough liquid superheat around the bubble to sustain its growth [9,25]. Thus, it is assumed in this study that the liquid in the bubbly layer is superheated and the top of the bubbly layer is at the saturation temperature. The top of the bubbly layer will represent the bottom boundary of the computational domain, as shown in Fig. 2. The intensity of the flow disturbances due to bubble dynamics is assumed to have a maximum value at this bottom boundary. The influence of the bubble-induced disturbances is assumed to decay with the normal distance from the top of the bubbly layer. The enhancement resulted from such disturbances is represented here by additional diffusion of momentum and energy that originate at the domain bottom boundary, i.e., at the top of the bubbly layer. In addition to the molecular diffusivity in the diffusion term of the conservation equations, an additional diffusivity has been added such that it accounts for the bubble-induced diffusion. Such diffusivity is not constant, it is rather assumed to decay in the vertical direction, as shown in Fig. 2. With that spatial variation in the normal direction and being dependant on the flow velocity and temperature, the additional diffusivity is, thus a flow property, not a fluid property. The momentum and energy equations are then solved within the computational domain of interest in order to obtain the flow and the temperature fields under the effect of the additional diffusion of momentum and heat from the bottom boundary. The ratio of the heat transfer from the bottom boundary and the amount of heat transfer calculated using the fluid molecular diffusivity only (no additional diffusion) is used here to represent the additional wall heat transfer due to bubble-induced diffusion, i.e., due to boiling.

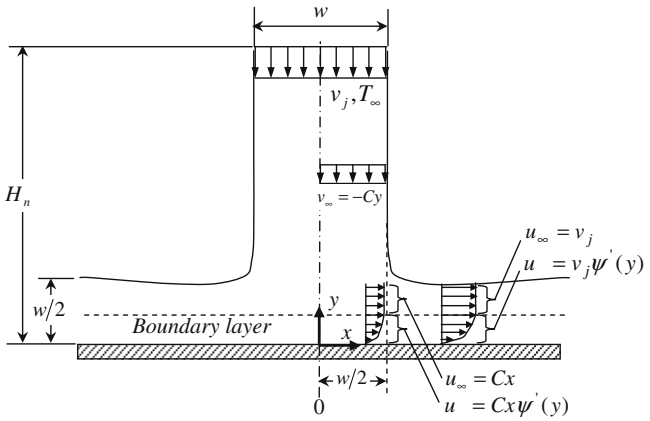

Fig. 1. Velocity field of an impinging planer jet $Cx\psi'(y)$.

3. The mathematical formulation

The following assumptions have been employed in this study:

1. Liquid properties are constant.
2. The flow is incompressible and steady.
3. The surface temperature in the stagnation region is constant. This assumption is valid given the size of the stagnation region considered in this study. This assumption permitted the use of classical stagnation flow solutions reported in [26].
4. The additional diffusivities in the momentum and in the energy equations are equal.
5. The additional diffusivities are decaying functions in the vertical direction.
6. The temperature at the bottom of the computational domain is equal to T_{sat}.
7. The amount of heat transfer due to evaporation is negligible. The validity of this assumption will be discussed later.
8. The boundary layer thickness in the stagnation region is assumed constant because of the balance between the flow acceleration and the viscous effect [26].

The boundary layer flow problem depicted in Fig. 2 can be mathematically represented by the following set of boundary layer equations:

1. The continuity equation:

$$\frac{\partial u}{\partial x} + \frac{\partial v}{\partial y} = 0 \tag{1}$$

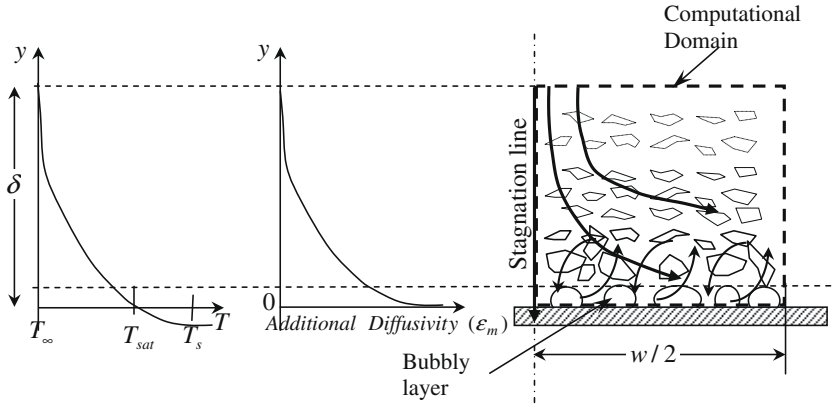

Fig. 2. Flow structure and the assumed temperature additional diffusivity profiles in the domain of interest.

2. The momentum equation:

$$u\frac{\partial u}{\partial x}+v\frac{\partial u}{\partial y}=-\frac{1}{\rho_l}\frac{dP}{dx}+\frac{\partial}{\partial y}\left[(\varepsilon_m+\nu)\frac{\partial u}{\partial y}\right] \tag{2}$$

3. The energy equation:

$$u\frac{\partial T}{\partial x}+v\frac{\partial T}{\partial y}=\frac{\partial}{\partial y}\left[(\varepsilon_h+\alpha)\frac{\partial T}{\partial y}\right] \tag{3}$$

The total diffusivity in Eqs. (2) and (3) equals the sum of the additional diffusivity, ε, (due to the bubble-induced diffusion) and the molecular diffusivity. The additional diffusivity is assumed to have a maximum value at the bottom boundary of the computational domain, defined as: $\varepsilon_{max} = \varepsilon_{m,max} + \nu$. The ratio between the maximum total diffusivity to the molecular diffusivity is defined as $\varepsilon^+ = \varepsilon_{max}/\nu$. Similar description of the enhanced thermal diffusivity has been used. According to assumption number (4), the bubble-induced diffusion Prandtl number, $Pr_t = \varepsilon_m/\varepsilon_h$ is assumed = 1.

The velocity components can be defined in terms of a stream function $\psi(y)$. In the stagnation region, the velocity components u and v in the x- and y-directions can be represented as [3,4,26]:

$$u = Cx\psi'(y) \tag{4a}$$
$$v = -C\psi(y) \tag{4b}$$

The velocity gradient C is expressed in terms of the jet velocity and the jet width [3] as $C = \overline{C}v_j/w$, where the value of $\overline{C} \sim 1.0$ [3,4].

The pressure distribution in the outer region of the flow is given by the Bernoulli's equation as:

$$P_o - P = \frac{1}{2}\rho_l C^2[x^2 + F(y)] \tag{5}$$

where P_o is the stagnation pressure. It should be noticed here that only the gradient of pressure parallel to the surface; $\partial P/\partial x$ is needed for the solution of the conservation equations. Therefore, the evaluation of the function $F(y)$ is not necessary in this context. Combining Eqs. (4) and (5) together with the definition of ε, the momentum and the energy equations can be written as:

$$\frac{\varepsilon}{C}\psi''' + \left(\frac{\varepsilon'}{C}+\psi\right)\psi'' - (\psi')^2 + 1 = 0 \tag{6}$$

$$\frac{\varepsilon}{C}\frac{\partial^2 T}{\partial y^2} + \left(Pr_t\,\psi + \frac{\varepsilon'}{C}\right)\frac{\partial T}{\partial y} = 0 \tag{7}$$

Introducing a set of dimensionless variables for the coordinates x and y, the stream function $\psi(y)$, the velocity components u and v, and the temperature T:

$$\eta = y\sqrt{\frac{C}{\varepsilon_{max}}},\quad \Psi = \psi\sqrt{\frac{C}{\varepsilon_{max}}},\quad \bar{x} = \frac{x}{w},\quad \bar{u} = \frac{u}{v_j},\quad \bar{v} = \frac{v}{v_j},$$
$$\theta = \frac{T - T_\infty}{T_{sat} - T_\infty}$$

Eqs. (6) and (7) can be written in dimensionless form as:

$$N\Psi''' + N'\Psi'' + \Psi\Psi'' - (\Psi')^2 + 1 = 0 \tag{8}$$
$$N\theta'' + (Pr_t\,\Psi + N')\theta' = 0 \tag{9}$$

where N is defined as $N(\eta) = \varepsilon/\varepsilon_{max}$. This function of the additional diffusivity should satisfy the hypothesis of the decaying diffusivity with the vertical distance. $N(\eta)$ has been assumed in the following form [3,4]:

$$N = \frac{\varepsilon_m + \nu}{\varepsilon_{max}} = \exp(-c_\varepsilon\eta) + \frac{\nu}{\varepsilon_{max}} = \exp(-c_\varepsilon\eta) + \frac{1}{\varepsilon^+} \tag{10}$$

where c_ε has been assumed ≈2 [4]. The boundary conditions for Eqs. (8) and (9) are:

$$\eta = 0:\ \Psi = \Psi' = 0,\quad \theta = 1,\quad N = 1 \tag{11a}$$
$$\eta \to \infty:\ \Psi' \to 1,\quad \theta, N \to 0 \tag{11b}$$

The solution of Eqs. (8) and (9); where all derivatives are with respect to η, provides information on the variation of Ψ and θ across the boundary layer as affected by the bubbles activity.

It is a known characteristic of the above system of ODEs (Eqs. (8) and (9)) that it is very sensitive to the boundary values $\Psi''(0)$ and $\theta'(0)$ [22,26]. In this study, as the bubble activity changes, it induces corresponding changes in the additional diffusion and hence the value of ε^+ is changed. The values of $\Psi''(0)$ and $\theta'(0)$ at the lower boundary of the domain of interest would also change accordingly to keep the upper boundary conditions (11b) satisfied. For this purpose, an iterative solution procedure has been developed using the Runge–Kutta method and Matlab® to obtain the corresponding values of Ψ'' and θ' at $\eta = 0$ that would satisfy the upper boundary conditions for a given value of ε^+. Table 1 shows the variation in these values with ε^+.

Fig. 3 shows some typical results with $\varepsilon^+ = 10$. It is evident from table 1 and Fig. 3 that the values of $\Psi''(0)$ and $\theta'(0)$ needed to be adjusted to the fifth or sixth digit to satisfy the top boundary conditions.

When the value of the first derivative of the dimensionless temperature $\theta'(0)$ is determined at the lower boundary of the domain of interest, the heat flux transferred to the bulk flow as a result of the enhanced bubble-induced diffusion can be obtained from:

$$q''_{nb,model} = \rho_l c_p \varepsilon_{max}\left(\frac{\partial T}{\partial y}\right)_{y=0} = \rho_l c_p (T_{sat} - T_\infty)\sqrt{\varepsilon_{max} C}\left(\frac{d\theta}{d\eta}\right)_{\eta=0} \tag{12}$$

Table 1
Values of $\Psi''(0)$ and $\theta'(0)$ obtained at different ε^+ values.

ε^+	$\Psi''(0)$	$\theta'(0)$
1	0.732978	0.313005
3	0.826835	0.32555
5	0.846944	0.32542
10	0.861121	0.31905
25	0.868753	0.31162
50	0.871068	0.30948
100	0.872174	0.30802
250	0.872818	0.3075
500	0.87303	0.3073
1000	0.873135	0.3071

In Eq. (12), the effects of the jet velocity and the surface superheat on the additional diffusion are accounted for in the value of ε_{max}, which in turns affects the temperature gradient at the bubbly layer, and hence affects the value of boiling heat flux. The solution flowchart to obtain the theoretical values of the wall heat flux due to the bubble-induced diffusion is shown in Fig. 4.

To estimate the total heat flux from the wall to the jet flow, the nucleate boiling heat flux calculated from Eq. (12) is added to the single heat flux due to forced convection. Several correlations were reported in the literature to calculate the stagnation heat transfer coefficient [27]. Those relations were tested against the experimental results of the current study in the single phase regime and the following relationship was found to best fit the results:

$$h_{sp} = 0.505\, Re_w^{0.5}\, Pr_l^{0.376}\, \frac{k_l}{w} \tag{13}$$

Single phase heat transfer is determined from:

$$q''_{sp} = h_{sp}(T_s - T_\infty) \tag{14}$$

So, the total wall flux is thus the sum of both parts:

$$q''_w = q''_{sp} + q''_{nb} \tag{15}$$

Eq. (12) can be rearranged to obtain the following expression for the nucleate boiling heat flux as function of dimensionless total diffusivity ε^+:

$$q''_{nb,model} = (\varepsilon^+)^{0.5} \rho_l c_p (T_{sat} - T_\infty) \sqrt{\frac{\overline{C} V_j \nu}{w}} \left(\frac{d\theta}{d\eta}\right)_{\eta=0} \tag{16}$$

Fig. 5 shows variation of the nucleate boiling heat flux with the dimensionless total diffusivity ε^+ at various values of jet velocity and degree of sub-cooling listed in Table 2. Results indicate that a certain value of surface heat flux can be achieved using various combinations of liquid sub-cooling and jet velocity. The effect of increasing jet velocity could be alleviated by decreasing degree of sub-cooling, so that boiling intensity would be maintained at the same level.

Eq. (12) together with the iterative solution of Eqs. (8) and (9) to obtain $\theta'(0)$ forms a procedure to predict the surface heat flux provided that the bubble-induced diffusivity is pre-determined in addition to the jet flow conditions.

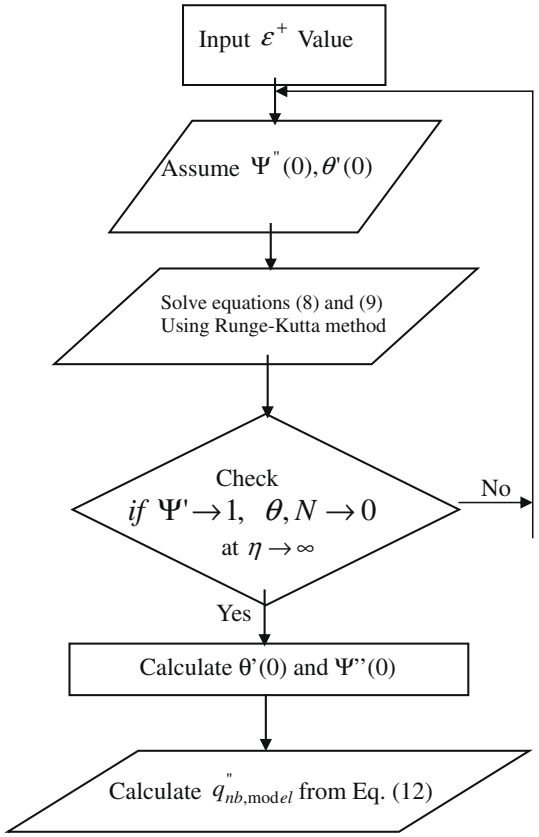

Fig. 4. Flow chart of the analytical part of the proposed model.

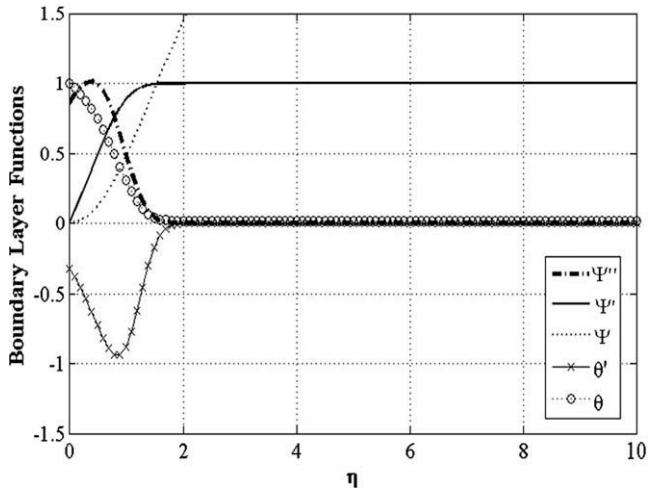

Fig. 3. Analytical solution of the dimensionless functions within the boundary layer. Case of $Pr_t = 1,\ \varepsilon^+ = 10,\ H''(0) = \Psi'''(0),\ \theta'(0) = -0.31895$.

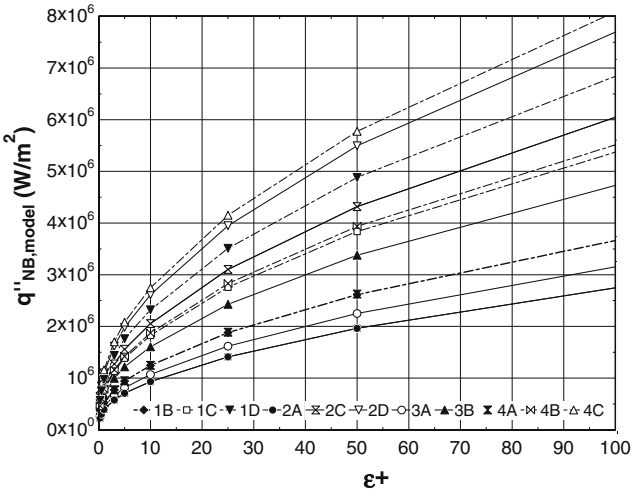

Fig. 5. Variation of $q''_{nb,model}$ with ε^+ at different flow conditions. Numbers and letters refer to velocity and degree of sub-cooling values listed in Table 2.

Table 2
Values of the jet velocity and the degree of sub-cooling considered in the experiments.

Velocity level	V_j (m/s)	Sub-cooling level	ΔT_{sub} (°C)
1	0.75	A	10
2	0.95	B	15
3	1.3	C	22
4	1.7	D	28

4. Model closure

Since the bubble induced diffusivity is not known a priori, it cannot be used as an input to predict the surface heat flux. Therefore, the model would still need a correlation between the practical inputs (i.e., the surface temperature, the jet velocity, and the liquid temperature) on one hand and the corresponding additional diffusivity on the other hand, which can then be used as an input to the model as shown in Fig. 4 to determine the surface heat flux. A set of experiments has been carried out in order to obtain enough data to use regression analysis to develop such a correlation. Table 2 summarizes the range of jet velocity and degree of sub-cooling used in the experiments.

4.1. Description of the experimental setup

Fig. 6a is a schematic illustration of the experimental apparatus. The heated surface is the top surface of a pure copper plate heated indirectly using a DC power supply. The current passes through a 25 μm thick NiCr 80/20 foil placed beneath the copper block to provide steady heat input to the surface. Constant temperature levels were maintained by adjusting the heat input to the plate using proportional feedback control. A thin layer of electrical insulation was placed between the heater and the copper block. Fig. 6b shows the locations of the twelve type-K, 0.5 mm diameter, thermocouples embedded in the copper block. The thermocouples were placed at two rows below the exposed surface in order to measure the local temperature variation in the flow direction, from the stagnation point, over a distance of ten times the jet width. Readings of these thermocouples were used as boundary conditions for the two-dimensional, steady, finite difference analysis that was employed to obtain spatial variation of temperature and total wall heat flux at the surface. Details of this analysis have been reported elsewhere [28].

For stagnation flow, Lienhard [27] reported a critical Reynolds number ($Re_{w,c}$) of 4000; based on the jet width, for the transition from laminar to turbulent. The range of Reynolds number in the current study is less than $Re_{w,c}$ with the exception of the case of jet velocity = 1.7 m/s at which Re_w is 5100. The maximum value of local Reynolds number ($Re_{x=LH}$) downstream of the stagnation point is 51,000 which is less than the critical value for parallel flows of 3×10^5.

Visual images of the bubble diameter and area density have been obtained by using a high speed camera placed at one side of the heated surface. Images were recorded at the rate of 1000 frames per second and analysed using an image-processing algorithm and the ImageJ software. The recorded images were decomposed into *stack* of gray scale images, as shown in Fig. 7. The images in the stack were subjected to carefully selected filters to sharpen the bubble edges before measuring the diameter. The images were then converted into monochromatic black and white pictures with the selection of the proper threshold of the gray scale. Bubble circularity and size were chosen after an intensive check of the frames within the stack to avoid the identification of light reflections from the free surface as bubbles. In the current study, the departure diameter of the bubbles was taken as the mean bubble diameter obtained from the entire stack.

Local measurements of the bubble release frequency have been conducted using an intrusive optical probe placed on the other side of the heated surface, as shown in Fig. 6a. An optical fibre is held in

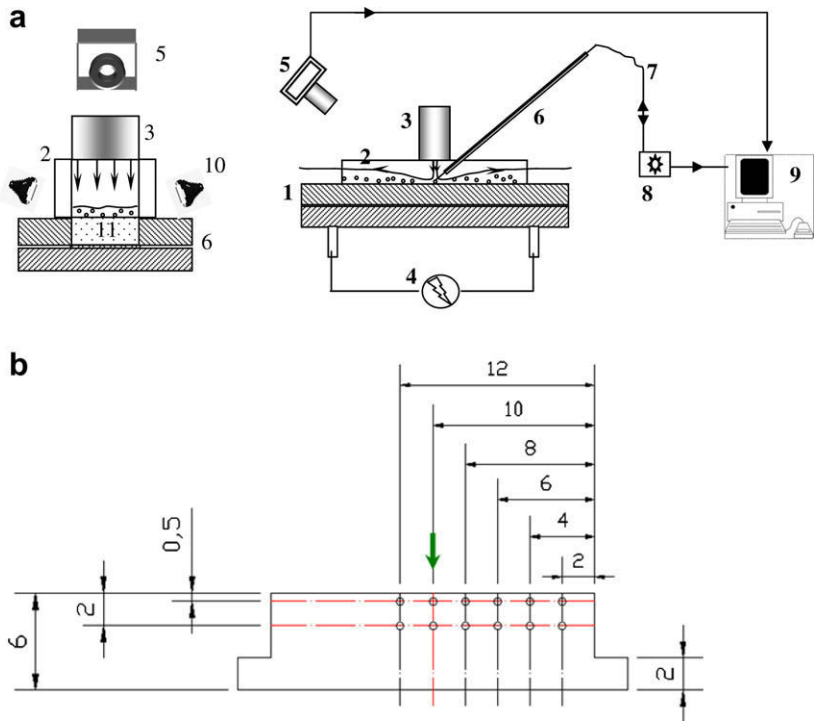

Fig. 6. (a) Schematic of the heated surface and instrumentation: (1) ceramic plates, (2) side glass, (3) planar nozzle, (4) DC power supply, (5) high speed camera, (6) stainless steel tube, (7) single mode optical fibre, (8) laser transceiver equipment, (9) PC, (10) light source, (11) the heated surface. (b) Locations of the thermocouples inside the test block. All dimensions are in mm. The thick arrow indicates location of the jet center.

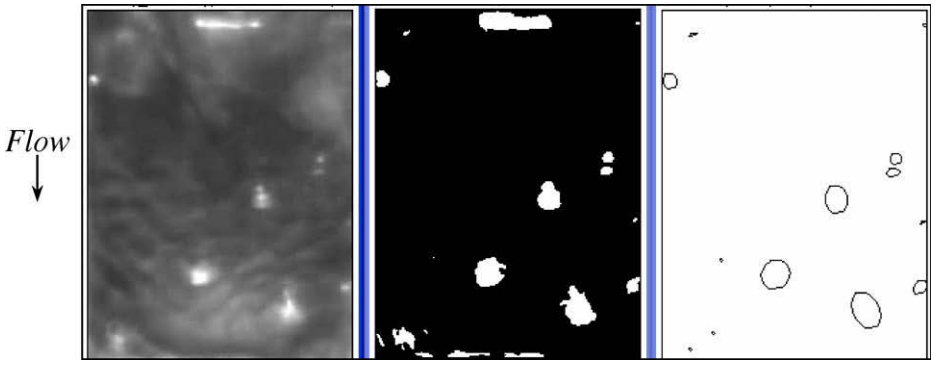

Fig. 7. Image processing procedure: (1) original pictures (left), (2) processed black and white pictures (middle), and (3) final with ellipses representing bubbles (right).

place using a steel tube maintaining a straight length of the fibre of 0.2 m with 10 mm of the probe tip protruding towards the surface. The tube is mounted on an XYZ micrometer in order to adjust probe location on the surface. As illustrated in Fig. 8, the number of vapour spikes per unit time was used to determine the bubble release frequency. A sampling frequency of 250 kHz was used to measure the vapour contact time and the frequency of bubble release at several nucleation sites (at least three) along the stagnation line. Bubble frequency in each experiment was obtained by averaging the frequency readings at three locations.

The estimated uncertainty in the experiments is: ±0.25 °C in the interior and surface temperatures, ±0.5 °C in the water temperature, ±5.2% in the wall heat flux, ±2.5% in the jet velocity, ±2% in the release frequency, ±25% in the bubble diameter.

4.2. Boiling curves

Sample boiling curves obtained at the stagnation for two levels of sub-cooling are shown in Fig. 9. The onset of nucleate boiling (ONB) is defined as the degree of superheat at which the two slopes of the boiling curve intersect, denoted by points B and D in Fig. 9. Results indicate that increasing the degree of sub-cooling from 15 to 28 °C resulted in a noticeable increase in the rate of heat transfer and a delay in the onset of nucleate boiling. The boiling curve has shifted upward in the case higher degree of sub-cooling indicating a positive effect of the sub-cooling on the single-phase heat flux and, to a less extent, on the nucleate boiling heat flux.

4.3. Determination of bubble dynamics

The bubble dynamics is characterised by the bubble diameter and the bubble release frequency. Both parameters affect the intensity of the additional diffusion caused by bubble-induced mixing. The current experimental results showed that both variables are affected by the jet velocity, the degree of sub-cooling, and the degree of surface superheat. Dimensional analysis revealed that the additional diffusivity is function of the following dimensionless numbers:

$$Re_b = \frac{V_j D_b}{\nu}, \quad We_b = \frac{\rho V_j^2 D_b}{\sigma}, \quad Ja_{sup} = \frac{\rho_l c_p (T_s - T_{sat})}{\rho_v h_{fg}},$$
$$Ja_{sub} = \frac{\rho_l c_p (T_{sat} - T_\infty)}{\rho_v h_{fg}} \tag{17}$$

The characteristic length used in the present study is the bubble diameter, and not the jet diameter. Several correlations for the bubble mean diameter as function of the surface and flow variables are available in the literature [29]. The following correlation, proposed by Basu et al. [15], has been used in the present study.

$$\frac{D_b}{L_c} = 1.3(\sin\phi)^{0.4}[0.13\exp(-1.75E-4Re_w) + 0.005]Ja_{sup}^{0.45} \times \exp(-0.0065Ja_{sub}) \tag{18}$$

where $L_c = \sqrt{\sigma/g(\rho_l - \rho_v)}$ and the contact angle between water and the copper surface is assumed $\phi \sim 50^\circ$ [15]. Eq. (18) was chosen because it includes all the important parameters of interest in this

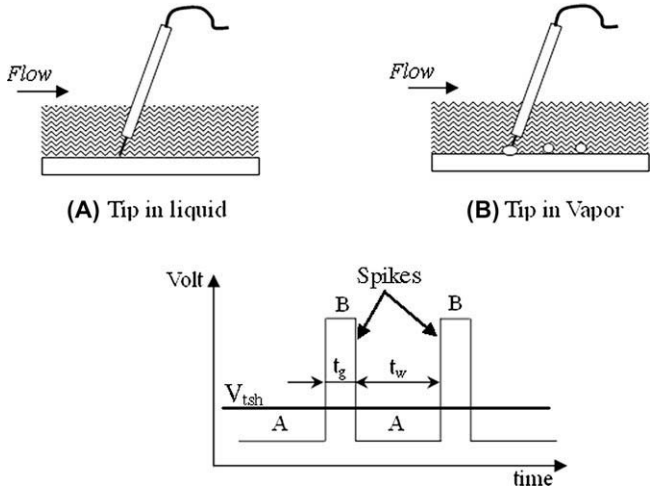

Fig. 8. Illustration of the operation of the intrusive optical probe showing the variation of probe signal with the fluid in contact.

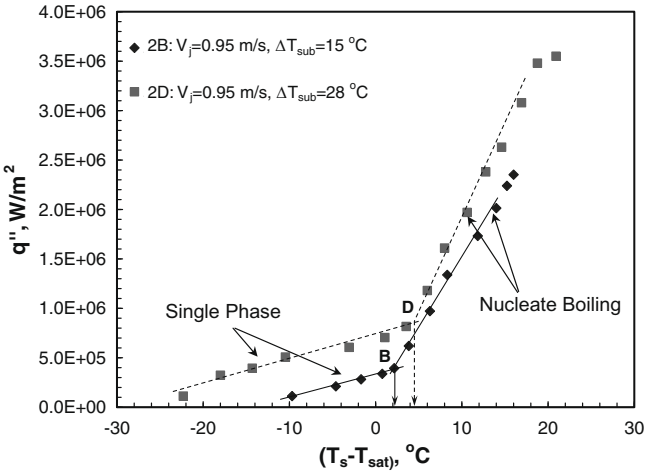

Fig. 9. Boiling curves showing the effect of degree of sub-cooling on the total flux at the stagnation point.

study. Its accuracy has been tested against the values of the mean bubble diameter calculated using the statistics obtained from the visual images, shown in Fig. 7. Fig. 10a shows the histogram of the bubble diameter obtained for case 1A, which is consistent with similar distributions reported in previous studies [15,30]. The range of the mean bubble diameter calculated under the conditions of the current study was $D_b \sim 0.1$–0.4 mm. The bubble diameter near the stagnation is closer to the lower limit.

Eq. (18) over predicted the mean bubble diameter, which was attributed to the fact that it did not account for the effect of jet impingement at the stagnation point. In order to include this effect, a modified gravitational acceleration term (g_{mod}) was introduced and used to calculate the characteristic length L_c. g_{mod} is defined by:

$$g_{mod} = g + \frac{V_j^2}{2d_{hyd}} \tag{19}$$

where d_{hyd} is the hydraulic diameter of the nozzle. Histograms of bubble diameter, bubble release frequency and percentage of area covered by bubbles are shown in Fig 10a, b and c, respectively. The release frequency, f, was in the range between 100 and 500 Hz. The bubble population density (N/A) was in the range between 10 and 50 bubbles/cm^2. Using the upper limits of these ranges, the amount of heat used to evaporate the liquid can be determined using Eq. (20).

$$q_{ev} = \rho_v \frac{\pi}{6} D_b^3 f \left(\frac{n}{A}\right) h_{fg} \tag{20}$$

where n is the active nucleation sites detected on the surface area A. This amount of heat was less than 1% of the total heat input, which justifies assumption number 7 in Section 3. Therefore, the only effect of bubble nucleation on the total amount of heat transfer is attributed to the additional agitation induced within the bubbly layer; not to the amount of heat required for evaporation (phase change).

4.4. Correlation of the enhanced (additional) diffusivity

For each experiment, i.e., for each combination of jet velocity, degree of sub-cooling, and degree of superheat, the development of the correlation between the model inputs and the additional diffusivity has been carried out according to the following procedure:

1. Determine the portion of the heat flux due to single-phase heat transfer, using Eq. (14).
2. The total heat flux to the surface is calculated from the finite-difference analysis [28].
3. The amount of heat transferred due to the nucleate boiling, q''_{nb} = the total wall flux minus the single-phase heat flux.
4. Calculate the additional diffusivity from Eq. (16).
5. Calculate the bubble diameter (D_b) at the corresponding wall temperature, jet velocity, and degree of sub-cooling from Eq. (18).
6. Calculate the dimensionless groups ($Re_b, We_b, Ja_{sup}, Ja_{sub}$) from Eq. (17).
7. Eq. (21), below, is the correlation obtained using regression analysis and the values of the dimensionless diffusivity (ε^+)

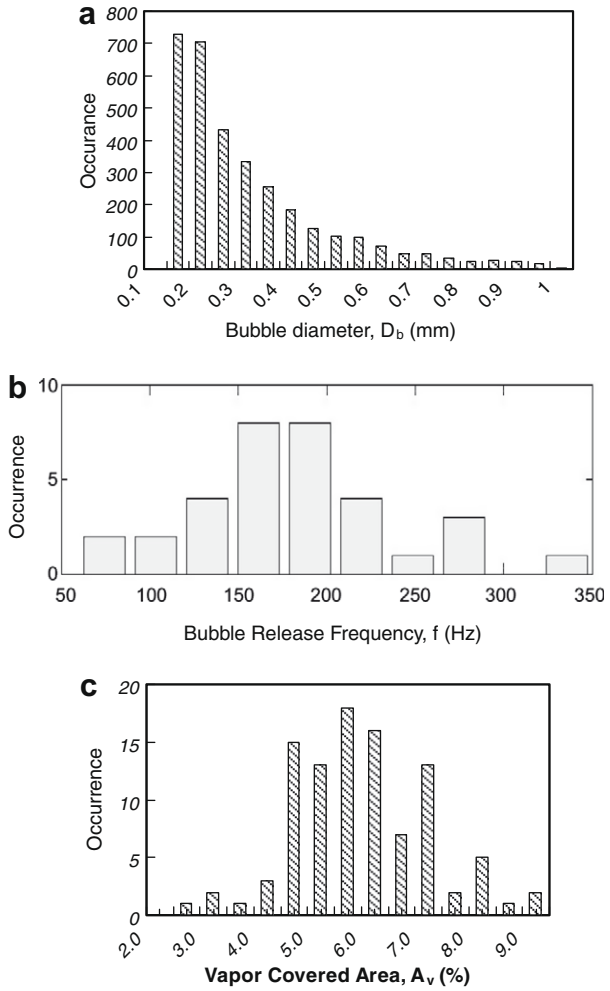

Fig. 10. Variation of (a) bubble diameter, (b) bubble release frequency, occurrence is the number of frames, 1 ms/frame, and (c) percentage of area covered by vapour, occurrence is number of sampling peroids, 100 ms/sample. Results are for case 1A and T_s = 115 °C.

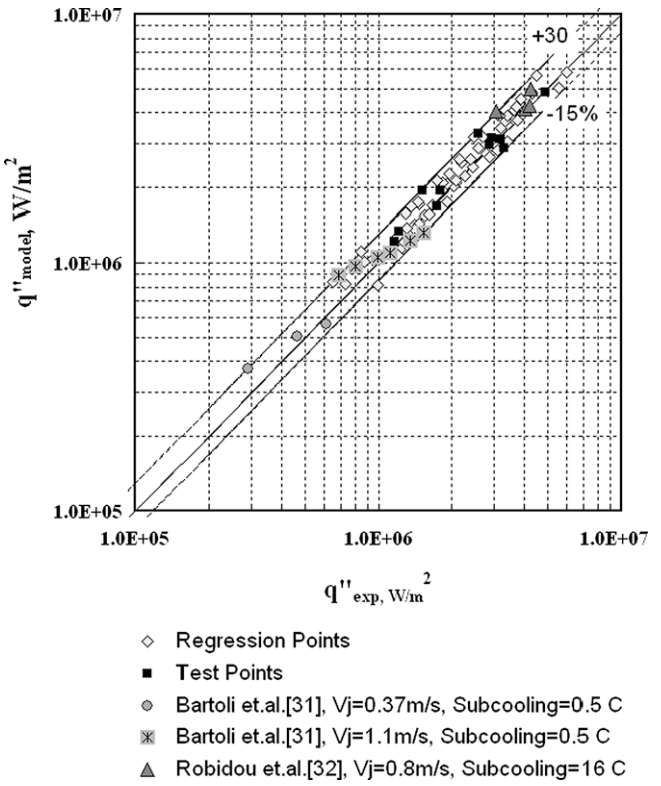

Fig. 11. Model predictions of the total wall heat flux. Black squares correspond to validation experiments.

Table 3
Particulars of the validation set.

V_j (m/s)	ΔT_{sub} (°C)	ΔT_{sat} (°C)	ε^+ (dimensionless)	q''_{exp} (MW/m^2)	q''_{model} (MW/m^2)	Variation %
0.4	21	12.5	10.89	1.53	1.95	+27
0.75	10	10.5	8.5	1.17	1.22	+4.27
0.75	15	20	38.2	3.22	3.13	-2.73
0.75	28	19.7	27.5	4.9	4.83	-1.47
0.95	10	17	21	1.8	1.95	+8.39
0.95	10	25	53.3	3.3	2.89	-12.33
0.95	15	11	12.7	1.74	1.675	-3.74
0.95	22	15.5	10.5	2.87	2.98	+3.73
0.95	28	14.5	7.62	2.6	3.3	+27
1.25	15	7.7	1.36	1.22	1.34	+9.75
1.25	15	22	19.9	2.93	3.17	+8.26

and the dimensionless groups (Re_b, We_b, Ja_{sup}, Ja_{sub}). Data from a set of 65 experiments were used for the development of this correlation.

$$\varepsilon^+ = \frac{Re_b^{x1}\, Ja_{sup}^{x4} Ja_{sub}^{x5}}{(We_b^{x2} + x_3)} \tag{21}$$

where: $x_1 = -0.7736$, $x_2 = 4.283$, $x_3 = 5.634$, $x_4 = 4.167$, $x_5 = -1.586$.

The values of the constants x_1 to x_5 in Eq. (21) reflect the effect of the different forces and flow conditions on the behaviour of the bubbles, and hence on the expected value of the additional diffusivity due to bubble-induced mixing. For example, according to Eq. (21), increasing the inertial forces, represented by the value of Re_b or increasing the degree of sub-cooling, represented by Ja_{sub}, would result in a lower diffusivity, which is in accordance with what is expected. Since these effects suppress bubble nucleation. On the contrary, an increase in the degree of wall superheat, represented by Ja_{sup}, causes the bubbles to nucleate at a higher frequency and grow to larger diameters, as suggested by Eq. (18), which result into a higher bubble-induced diffusivity, in agreement with Eq. (21).

4.5. Prediction of the surface heat flux using the proposed model

The procedure to predict the total boiling heat flux using the proposed model is as follows:

1. Calculate the additional diffusivity for any combination of the input parameters (jet velocity, degree of sub-cooling, and degree of superheat) using Eq. (21).
2. Using the analytical model, see Fig. 4, obtain the value of $\theta'(0)$.
3. The value of the nucleate boiling heat flux is calculated from Eq. (12).
4. The single-phase heat flux is obtained from Eqs. (13) and (14).
5. Finally, the total wall heat flux is calculated from Eq. (15).

5. Model accuracy and validation

Fig. 11 shows the variation of the predicted total wall heat flux and the measured values for all 65 data points used in the present study. The Fig. shows that the predictions are in reasonable agreement with the experimental results. The overall variation of the predicted values is in the range of +30% and −15% for all conditions considered in this study.

The model was validated using inputs corresponding to a separate set of 11 validation experiments that was not included in the regression analysis. Table 3 lists the particulars of these experiments. The solid squares shown in Fig. 11 are the predictions corresponding to this validation set. These predictions were well within the same overall range of accuracy reported above.

Predictions of the proposed model have also been compared with experimental data reported in previous investigations [31,32]. Bartoli et al. [31] carried out a set of steady-state experiments of boiling heat transfer in the stagnation zone of a planner jet impinging on the side of a stainless steel cylinder. Robidou et al. [32] conducted a set of steady-state experiments of boiling heat transfer of a planer jet impinging on a horizontal flat surface. Results shown in Fig 11 indicate that the proposed model is capable of predicting the stagnation heat flux in these experiments within the same overall range of accuracy reported above.

6. Summary and conclusions

A new model to predict the total wall heat flux in the stagnation region of a free planar jet impinging on a flat surface has been developed. The model utilizes the concept of additional diffusion due to bubble-induced mixing. A set of experiments has been carried out in order to develop the required correlation between the additional diffusivity and the jet velocity, the degree of sub-cooling, and the degree of surface superheat.

The model has been validated using additional sets of experimental data and three sets of data from previous studies. The predictions of the surface heat flux using the proposed model are within the typical range of variation reported in other boiling heat transfer studies.

Incorporating the proposed model in numerical simulations of boiling heat transfer would allow one to include the effect of boiling on the flow and thermal fields using the concept of additional diffusion without the need to resolve all the details of the two-phase flow associated with the boiling. This approach would result in significant reduction in the cost of boiling heat transfer simulations.

Acknowledgements

The authors would like to acknowledge the financial support of this research received from the Natural Sciences and Engineering Research Council of Canada (NSERC).

References

[1] D.H. Wolf, F.P. Incropera, R. Viskanta, Jet Impingement Boiling, Adv. Heat Transfer 23 (1993) 1–132.
[2] Z. Liu, J. Wang, Study on film boiling heat transfer for water jet impinging on high temperature flat plate, Int. J. Heat Mass Transfer 44 (2001) 2475–2481.
[3] D.A. Zumbrunnen, Convective heat and mass transfer in the stagnation region of a laminar planar jet impinging on a moving surface, J. Heat Transfer 113 (1991) 563–570.
[4] W. Timm, K. Weinzierl, A. Leipertz, Heat transfer in subcooled jet impingement boiling at high wall temperature, Int. J. Heat Mass Transfer 46 (2003) 1385–1393.
[5] D.E. Hall, F.P. Incropera, R. Viskanta, Jet impingement boiling from a circular free-surface jet during quenching: part 1 – single-phase jet, J. Heat Transfer 123 (2001) 901–910.

[6] M.S. Hamed, M. Akmal, Determination of heat transfer rates in an industry-like spray quench system using multiple impinging water jets, Int. J. Mater. Prod. Technol. 24 (3/4) (2005) 184–198.
[7] C.F. Ma, A.E. Bergles, Jet impingement nucleate boiling, Int. J. Heat Mass Transfer 29 (8) (1986) 1095–1101.
[8] A.O., Tay, H., Xue, C. Yang, Cooling of electronic components with free jet impingement boiling, in: Inter Society Conference on Thermal Phenomena, IEEE, 2002, pp. 387–394.
[9] V.P. Carey, Liquid–Vapor Phase-Change Phenomena, Series in Chemical and Mechanical Engineering, Taylor & Francis, London, 1992.
[10] Y. Katto, M. Shimizu, Upper limit of CHF in the saturated forced convection boiling on a heated disk with a small impinging jet, J. Heat Transfer 101 (1979) 265–269.
[11] Y. Katto, S. Yokoya, Critical heat flux on a disk heater cooled by a circular jet of saturated liquid impinging at the center, Int. J. Heat Mass Transfer 31 (2) (1988) 219–227.
[12] G.R. Warrier, V.K. Dhir, Heat transfer and wall heat flux partitioning during subcooled flow nucleate boiling – a review, J. Heat Transfer 128 (2006) 1243–1255.
[13] R.L. Judd, H. Merte Jr., Evaluation of nucleate boiling heat flux predictions at varying levels of subcooling and acceleration, Int. J. Heat Mass Transfer 15 (1972) 1075–1096.
[14] R.L. Judd, K.S. Hwang, Comprehensive model for nucleate pool boiling heat transfer including microlayer evaporation, J. Heat Transfer 98 (4) (1976) 623–629.
[15] N. Basu, G. Warrier, V.K. Dhir, Wall heat flux partitioning during flow boiling: part I: model development, J. Heat Transfer 127 (2005) 131–140.
[16] H. Steiner, A. Kobor, L. Gebhard, A wall heat transfer model for subcooled boiling flow, Int. J. Heat Mass Transfer 48 (2005) 4161–4173.
[17] J. Shu, G. Wilks, Heat transfer in the flow of a cold, two-dimensional vertical liquid jet against a hot, horizontal plate, Int. J. Heat Mass Transfer 39 (16) (1996) 3367–3379.
[18] X.S. Wang, Z. Dagan, L.M. Jiji, Heat transfer between a circular free impinging jet and a solid surface with non-uniform wall temperature or wall heat flux – 1: solution for the stagnation region, Int. J. Heat Mass Transfer 33 (7) (1989) 1351–1360.
[19] M. Mat, Y. Kaplan, O. Ilegbusi, Application of a bubble-induced turbulence model to subcooled boiling in a vertical pipe, MD-Vol.89, The Science, Automation, and Control of Material Processes Involving Coupled Transport and Rheology Changes, ASME, 1999.
[20] J. Mikielewicz, D. Mikielewicz, D. Barnik, Modeling of nucleate boiling heat transfer in a film formed by an impingement jet, Heat Transfer Res. 38 (4) (2007) 313–323.
[21] H. Tennekes, J.L. Lumley, A First Course in Turbulence, MIT Press, Cambridge, MA, 1972.
[22] W. Timm, Personal communications, 2007. Regarding the topic in [4].
[23] V.K. Dhir, H.S. Abarajith, D. Li, Bubble dynamics and heat transfer during pool and flow boiling, Heat Transfer Eng. 28 (7) (2007) 608–624.
[24] S. Narumanchi, A. Troshko, D. Bharathan, V. Hassani, Numerical simulations of nucleate boiling in impinging jets: applications in power electronic cooling, Int. J. Heat Mass Transfer 51 (1-2) (2008) 1–12.
[25] Y.Y. Hsu, On the size range of active nucleation cavities on a heating surface, J. Heat Transfer 84 (1962) 207.
[26] F.M. White, Viscous Fluid Flow, second ed., McGraw-Hill, New York, 1991.
[27] J.H. Lienhard V, Liquid jet impingement, Ann. Rev. Heat Transfer 6 (4) (1995) 199–270.
[28] A.M.T. Omar, M.S. Hamed, M. Shoukri, Experimental study of steady state nucleate boiling heat transfer under planar jet impingement, in: The 12th International Topical Meeting on Nuclear Reactor Thermal Hydraulics (NURETH-12), Sheraton Station Square, Pittsburgh, Pennsylvania, USA, September 30 – October 4, 2007.
[29] R.M. Podowski, D.A. Drew, R.T. Lahey Jr., M.Z. Podowski, A mechanistic model of the ebullition cycle in forced convection subcooled boiling, in: Proceedings of the 8th International Topical Meeting on Nuclear Reactor Thermal-Hydraulics, Koyoto-Japan, September 30 – October 4, 1997, pp. 1535–1542.
[30] V. Prodanovic, D. Frase, M. Salcudean, On the transition from partial to fully developed subcooled flow boiling, Int. J. Heat Mass Transfer 45 (2002) 4727–4738.
[31] C. Bartoli, P. Di Marco, S. Faggiani, Heat transfer and flow pattern at a cylinder impinged by a slot jet during incipient and nucleate boiling, Exp. Therm. Fluid Sci. 15 (1997) 101–108.
[32] H. Robidou, H. Auracher, P. Gardin, M. Lebouche, Controlled cooling of a hot plate with a water jet, Exp. Therm. Fluid Sci. 26 (2002) 123–129.